31st Congress of the International Council of the Aeronautical Sciences

Belo Horizonte, Brazil; September 09-14, 2018

ON REAL–TIME SIMULATION OF FLEXIBLE AIRCRAFT WITH PHYSICS–DERIVED MODELS

Paulino, J.A.* , **Da Ronch, A.**** , **Guimarães Neto, A.B.*** , **Silvestre, F.J.*** , **Morales, M.A.V.***
*Instituto Tecnológico de Aeronáutica, São José dos Campos, SP, 12228-900, Brazil ,
**University of Southampton, Southampton, SO171BJ, UK

Keywords: *flexible aircraft, aeroelasticity, simulation, reduced-order modeling*

Abstract

Flight simulation of flexible aircraft is computationally expensive. This paper presents an approach based on reduced–order models for computational cost reduction of the aeroelastic equations. The model order reduction technique, the X–HALE aircraft and a low computational cost model are described. Finally, simulation time histories are presented comparing time responses and computational costs. Numerical results show good agreement between full-order and reduced-order models, with the latter presenting a significant reduction in computational time.

1 Introduction

The development of modern, more efficiency transport aircraft and high altitude long endurance (HALE) aircraft requires light and flexible structures. At this point, the rigid–body assumption may not be accurate anymore and aeroelastic modes must be taken into account when modeling flight dynamics.

However, flight simulations of flexible aircraft are computationally expensive. The interaction between aerodynamics, structural dynamics and flight dynamics results in mathematical models with many state variables and nonlinear equations [1,2]. Even approaches based on linear structural and aerodynamic models can be expensive depending on the effects they represent [3].

In particular, real–time simulation of flexible aircraft is currently a challenge. The benefits provided by flight simulation are beyond design. Development costs are reduced by using flight simulators instead of flying prototypes, safety is increased by providing pilots training or by simulating situations that would be dangerous to be reproduced in real flight.

Real–time flight simulators can be used for control system validation via hardware–in–the–loop simulations [4,5]. They can also be used to perform pilot–in–the–loop simulations for evaluating handling qualities of an aircraft [6] or to investigate pilot–induced oscillations [7].

Motivated by the benefits of real–time simulation, this paper describes an approach for reducing computational cost of flexible aircraft models and presents preliminary results.

2 Model order reduction technique

The model order reduction technique employed in the current work was developed by Da Ronch et al [8]. It was conceived for flight control law design of flexible aircraft. In summary, the technique uses information on the eigenspectrum of the Jacobian matrix and projects the system through a Taylor series expansion onto a small basis of eigenvectors representative of the system dynamics, retaining terms up to second or third order.

Consider a flexible aircraft with dynamics represented by the state equation

$$\dot{\boldsymbol{x}} = \boldsymbol{F}(\boldsymbol{x}, \boldsymbol{u}), \tag{1}$$

where $\boldsymbol{F}$ is a nonlinear function, $\boldsymbol{u}$ is the con-

trol input vector and $\boldsymbol{x}$ is an n–dimensional state vector containing rigid–body, structural and fluid state variables:

$$\boldsymbol{x} = \begin{bmatrix} \boldsymbol{x}_{rb} \\ \boldsymbol{x}_{s} \\ \boldsymbol{x}_{f} \end{bmatrix}_{n\times 1}. \tag{2}$$

Consider now $\Delta\boldsymbol{x} = \boldsymbol{x} - \boldsymbol{x_0}$ a small perturbation in the state vector with respect to an equilibrium point $\boldsymbol{x_0}$ and $\Delta\boldsymbol{u} = \boldsymbol{u} - \boldsymbol{u_0}$ a small perturbation in the control input vector with respect to the equilibrium point $\boldsymbol{u_0}$. The nonlinear state equation represented by Eq. (1) is expanded in a Taylor series around $\boldsymbol{x_0}$ and $\boldsymbol{u_0}$ and the system dynamics is approximated by

$$\begin{aligned} \Delta\dot{\boldsymbol{x}} \approx \boldsymbol{A}\Delta\boldsymbol{x} + \frac{\partial \boldsymbol{F}}{\partial \boldsymbol{u}}\Delta\boldsymbol{u} + \frac{1}{2!}\boldsymbol{B}(\Delta\boldsymbol{x},\Delta\boldsymbol{x}) \\ + \frac{1}{3!}\boldsymbol{C}(\Delta\boldsymbol{x},\Delta\boldsymbol{x},\Delta\boldsymbol{x}), \end{aligned} \tag{3}$$

where $\boldsymbol{A}$, $\boldsymbol{B}$ and $\boldsymbol{C}$ represents the first, second and third Jacobian operators defined by

$$A_{ij} = \frac{\partial F_i(\boldsymbol{x_0})}{\partial x_j}, \tag{4}$$

$$B_i(\boldsymbol{a},\boldsymbol{b}) = \sum_{j,k=1}^{n} \frac{\partial^2 F_i(\boldsymbol{x_0})}{\partial x_j \partial x_k} a_j b_k, \tag{5}$$

$$C_i(\boldsymbol{a},\boldsymbol{b},\boldsymbol{c}) = \sum_{j,k,l=1}^{n} \frac{\partial^3 F_i(\boldsymbol{x_0})}{\partial x_j \partial x_k \partial x_l} a_j b_k c_l. \tag{6}$$

The Taylor series expansion (3) must be projected onto a small basis formed by m ($m \ll n$) eigenvectors of the Jacobian matrix $\boldsymbol{A}$ which are representative of the aircraft dynamics. Denote $\boldsymbol{\phi_i}$ and $\boldsymbol{\psi_i}$ the right and left eigenvectors of $\boldsymbol{A}$, i.e.

$$\boldsymbol{A}\boldsymbol{\phi_i} = \lambda_i \boldsymbol{\phi_i}, \quad \text{for } i = 1,\ldots,n, \tag{7}$$

$$\boldsymbol{A}^T\boldsymbol{\psi_i} = \bar{\lambda}_i \boldsymbol{\psi_i}, \quad \text{for } i = 1,\ldots,n. \tag{8}$$

It is convenient that the set of eigenvectors that forms the reduced–order model basis satisfies the biorthonormality conditions, i.e.

$$\langle \boldsymbol{\phi_i}, \boldsymbol{\phi_i} \rangle = 1, \quad \text{for } i = 1,\ldots,m, \tag{9}$$

$$\langle \boldsymbol{\psi_j}, \boldsymbol{\phi_i} \rangle = \delta_{ij}, \quad \text{for } i = 1,\ldots,m, \tag{10}$$

$$\langle \boldsymbol{\psi_j}, \bar{\boldsymbol{\phi}}_i \rangle = 0, \quad \text{for } i = 1,\ldots,m, \tag{11}$$

where δ_{ij} represents the Kronecker delta and the inner product is defined as $\langle \boldsymbol{a},\boldsymbol{b} \rangle = \bar{\boldsymbol{a}}^T\boldsymbol{b}$. Consider the transformation of coordinates

$$\Delta\boldsymbol{x} = \boldsymbol{\Phi}\boldsymbol{z} + \bar{\boldsymbol{\Phi}}\bar{\boldsymbol{z}}, \tag{12}$$

where

$$\boldsymbol{\Phi} = \begin{bmatrix} \boldsymbol{\phi_1} & \ldots & \boldsymbol{\phi_m} \end{bmatrix} \tag{13}$$

and $\boldsymbol{z} \in \mathbb{C}^m$ is the reduced–order model state variable vector. Applying the transformation of coordinates (12) into Eq. (3) and then premultiplying each term by the conjugate transpose of the left modal matrix, results in

$$\begin{aligned} \bar{\boldsymbol{\psi}}_j^T(\boldsymbol{\phi_i}\dot{z}_i + \bar{\boldsymbol{\phi}}_i\dot{\bar{z}}_i) = \bar{\boldsymbol{\psi}}_j^T\Big(\boldsymbol{A}\boldsymbol{\phi_i}z_i + \boldsymbol{A}\bar{\boldsymbol{\phi}}_i\bar{z}_i + \frac{\partial \boldsymbol{F}}{\partial \boldsymbol{u}}\Delta\boldsymbol{u} \\ + \frac{1}{2!}B_i(\boldsymbol{z},\boldsymbol{z}) + \frac{1}{3!}C_i(\boldsymbol{z},\boldsymbol{z},\boldsymbol{z})\Big). \end{aligned} \tag{14}$$

Once the biorthonormality conditions (9), (10) and (11) were satisfied, the set of m equations (14) can be simplified as

$$\begin{aligned} \dot{z}_i = \lambda_i z_i + \boldsymbol{\psi}_j^T\Big(\frac{\partial \boldsymbol{F}}{\partial u}\Delta\boldsymbol{u} + \frac{1}{2!}B_i(\boldsymbol{z},\boldsymbol{z}) + \\ \frac{1}{3!}C_i(\boldsymbol{z},\boldsymbol{z},\boldsymbol{z})\Big), \end{aligned} \tag{15}$$

where the bilinear and trilinear terms are written as

$$\begin{aligned} B_i(\boldsymbol{z},\boldsymbol{z}) = \sum_{r,s=1}^{m} B_i(\boldsymbol{\phi_r},\boldsymbol{\phi_s})z_r z_s + B_i(\boldsymbol{\phi_r},\bar{\boldsymbol{\phi}}_s)z_r\bar{z}_s + \\ B_i(\bar{\boldsymbol{\phi}}_r,\boldsymbol{\phi_s})\bar{z}_r z_s + B_i(\bar{\boldsymbol{\phi}}_r,\bar{\boldsymbol{\phi}}_s)\bar{z}_r\bar{z}_s \end{aligned} \tag{16}$$

and

$$
\begin{aligned}
C_i(\boldsymbol{z},\boldsymbol{z},\boldsymbol{z}) = \sum_{r,s,t=1}^{m} \Big(& C_i(\boldsymbol{\phi_r},\boldsymbol{\phi_s},\boldsymbol{\phi_t}) z_r z_s z_t + \\
& C_i(\boldsymbol{\phi_r},\boldsymbol{\phi_s},\bar{\boldsymbol{\phi}}_{\boldsymbol{t}}) z_r z_s \bar{z}_t + C_i(\boldsymbol{\phi_r},\bar{\boldsymbol{\phi}}_{\boldsymbol{s}},\boldsymbol{\phi_t}) z_r \bar{z}_s z_t + \\
& C_i(\boldsymbol{\phi_r},\bar{\boldsymbol{\phi}}_{\boldsymbol{s}},\bar{\boldsymbol{\phi}}_{\boldsymbol{t}}) z_r \bar{z}_s \bar{z}_t + C_i(\bar{\boldsymbol{\phi}}_{\boldsymbol{r}},\boldsymbol{\phi_s},\boldsymbol{\phi_t}) \bar{z}_r z_s z_t + \\
& C_i(\bar{\boldsymbol{\phi}}_{\boldsymbol{r}},\boldsymbol{\phi_s},\bar{\boldsymbol{\phi}}_{\boldsymbol{t}}) \bar{z}_r z_s \bar{z}_t + C_i(\bar{\boldsymbol{\phi}}_{\boldsymbol{r}},\bar{\boldsymbol{\phi}}_{\boldsymbol{s}},\boldsymbol{\phi_t}) \bar{z}_r \bar{z}_s z_t + \\
& C_i(\bar{\boldsymbol{\phi}}_{\boldsymbol{r}},\bar{\boldsymbol{\phi}}_{\boldsymbol{s}},\bar{\boldsymbol{\phi}}_{\boldsymbol{t}}) \bar{z}_r \bar{z}_s \bar{z}_t \Big)
\end{aligned} \tag{17}
$$

It is possible to calculate all the bilinear and trilinear contributions without calculating all the second and third order partial derivatives analytically. They can be approximated by using finite differences instead. The bilinear and trilinear contributions consist, in general, of $4m^2$ and $8m^3$ terms. However, it is possible to reduce the number of terms to $2m^2+m$ and $\frac{2}{3}(2m^3+3m^2+m)$ respectively by exploiting the symmetry of the Jacobian operators [8].

In this work, however, we calculate the derivatives by using automatic differentiation, a computational technique that takes advantage of the fact that every computer program executes a sequence of elementary operations. By applying the chain rule to these operations, it is possible to calculate the derivatives accurately without evaluating functions which are, in general, computationally expensive, and approximating the derivatives numerically, avoiding rounding and truncation errors. Since the aircraft model was implemented in *MATLAB*, *ADiGator* toolbox was used: a free, open source and easy–to–use automatic differentiation toolbox developed by Patterson et al [9].

3 X-HALE aircraft

The X–HALE (Figure 1) is a flexible, remotely piloted aircraft developed by Professor Carlos Cesnik and coworkers at the University of Michigan to provide a platform for collecting data that can be used in support for validation of coupled aeroelastic and flight dynamics formulations. It is also intended to be used as a platform for nonlinear control laws tests [10].

(a) X–HALE during flight tests at ITA

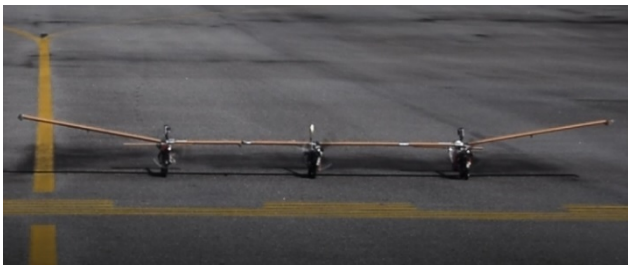

(b) X–HALE taxiing

Fig. 1 X–HALE aircraft

It is a wing–boom–tail aircraft designed to have a modular airframe that allows it to be mounted in three configurations: slightly flexible ($4m$ wingspan and aspect ratio equal to 20), moderately flexible ($6m$ wingspan and aspect ratio equal to 30) and highly flexible ($8m$ wingspan and aspect ratio equal to 40).

The wing profile is an EMX–07 reflexed airfoil with constant chord equal to $0.2m$ along the wingspan with an incidence angle equal to 5 degrees. In all three configurations, the outermost wing panels have 10 degrees dihedral angle and are equipped with trailing-edge control surfaces.

The tails comprise NACA–0012 symmetric airfoils with chord equal to $0.11m$. The central tail can be set to vertical or horizontal configuration only, to increase or decrease lateral–directional stability, respectively. The outer tails are always in the horizontal configuration and their incidence angle can be controlled.

The aircraft in its slightly flexible configuration (aspect ratio equal to 20) is currently in operation also at ITA in Brazil, and the moderately

configuration (aspect ratio equal to 30) will enter into operation in the near future.

In the current work, only the slightly flexible configuration (4m wingspan and aspect ratio equal to 20) is considered. Wing control surfaces are deflected antisymmetrically, working as ailerons. The central tail is set in vertical position during the entire simulations in order to increase lateral–directional stability. The outer tails are symmetrically deflected, working as elevators.

4 X-HALE model

The X–HALE model used in the current work was implemented following the methodology proposed by Silvestre [11], which was experimentally validated in flight for the utility aircraft Stemme S15 [12].

The representation of the flight dynamics including flexibility effects was based on the linearized mean–axes formulation, proposed by Waszak and Schmidt [13]. The equations of motion are detailed in Ref. [11] and reproduced here:

$$\dot{\boldsymbol{V}}|_B = -\boldsymbol{\omega}|_B \times \boldsymbol{V}|_B + \frac{1}{m}\left(\boldsymbol{T}_{BI}\boldsymbol{W}|_I + \boldsymbol{F}|_B\right) \quad (18)$$

$$\dot{\boldsymbol{\omega}}|_B = -\boldsymbol{J}^{-1}\left(\boldsymbol{\omega}|_B \times \boldsymbol{J}\boldsymbol{\omega}|_B\right) + \boldsymbol{J}^{-1}\boldsymbol{M}|_B \quad (19)$$

$$\dot{\boldsymbol{p}} = \boldsymbol{T}_{BI}^T \boldsymbol{V}|_B \quad (20)$$

$$\dot{\boldsymbol{\delta}} = -\boldsymbol{\tau}^{-1}\boldsymbol{\delta} + \boldsymbol{\tau}^{-1}\boldsymbol{u_c} \quad (21)$$

$$\begin{bmatrix}\dot{\boldsymbol{\eta}}(t)\\ \ddot{\boldsymbol{\eta}}(t)\end{bmatrix} = \begin{bmatrix}\boldsymbol{0}_{n_e\times n_e} & \boldsymbol{I}\\ \boldsymbol{\Pi_1}(t) & \boldsymbol{\Pi_2}(t)\end{bmatrix}\begin{bmatrix}\boldsymbol{\eta}(t)\\ \dot{\boldsymbol{\eta}}(t)\end{bmatrix} + \\ + \begin{bmatrix}\boldsymbol{0}_{n_e\times n_s}\\ \boldsymbol{\Pi_3}(t)\end{bmatrix}\boldsymbol{\lambda}(t) + \begin{bmatrix}\boldsymbol{0}_{n_e\times n_x}\\ \boldsymbol{\Pi_4}(t)\end{bmatrix}\boldsymbol{x}_{RB}(t) + \\ + \begin{bmatrix}\boldsymbol{0}_{n_e\times n_u}\\ \boldsymbol{\Pi_5}(t)\end{bmatrix}\boldsymbol{\delta}(t) \quad (22)$$

$$\dot{\boldsymbol{\lambda}} = \boldsymbol{\Lambda}(t)\boldsymbol{\lambda} + \boldsymbol{\Upsilon}\dot{\boldsymbol{w}}_{3/4}(t) \quad (23)$$

where $\boldsymbol{V}|_{\boldsymbol{B}}$ and $\boldsymbol{\omega}|_{\boldsymbol{B}}$ represents linear and angular velocities of the body reference frame with respect to the inertial reference frame; $\boldsymbol{T}_{BI}$ is the transformation matrix from the inertial frame to the body frame; m is the total mass of the aircraft; $\boldsymbol{W}|_{\boldsymbol{I}}$ is the aircraft weight expressed in the inertial reference frame; $\boldsymbol{J}$ is the inertia matrix with respect to the aircraft center of gravity; $\boldsymbol{p}$ is the position of the center of gravity with respect to the inertial frame; $\boldsymbol{\delta}$ is the state vector of the actuators; $\boldsymbol{\tau}$ is a diagonal matrix that contains the actuators' time constants; $\boldsymbol{u_c}$ is the control input; $\boldsymbol{\eta}$ is the vector of modal coordinates; $\boldsymbol{\lambda}$ is the aerodynamic lag vector and $\dot{\boldsymbol{w}}_{3/4}$ represents the first derivative of the downwash.

The length of the vectors $\boldsymbol{\eta}$ and $\boldsymbol{\lambda}$ are the number of elastic modes (n_e) and twice the the number of strips in the incremental aerodynamic model ($2n_s$), respectively. The matrices $\boldsymbol{\Pi_i}$ and $\boldsymbol{\Lambda}$ are time variant, depending on the flight condition and unsteady aerodynamics formulation. The matrix $\boldsymbol{\Upsilon}$ is constant and depends only on the coefficients of the exponential Jones approximation. The analytical definitions of those matrices can be found in Ref. [11].

$\boldsymbol{F}|_B$ and $\boldsymbol{M}|_B$ are the sum of external forces and moments, respectively, comprising rigid–body aerodynamics, incremental aeroelastic unsteady aerodynamics and propulsive forces and moments expressed in the body reference frame:

$$\boldsymbol{F}|_B = \boldsymbol{F}_{aero,RB}|_B + \boldsymbol{F}_{aero,incr}|_B + \boldsymbol{F}_{prop}|_B \quad (24)$$

$$\boldsymbol{M}|_B = \boldsymbol{M}_{aero,RB}|_B + \boldsymbol{M}_{aero,incr}|_B + \boldsymbol{M}_{prop}|_B \quad (25)$$

The rigid–body steady aerodynamic coefficients were calculated using Hedman's Vortex Lattice Method [14] and XFOIL [15]. They were disposed in lookup tables parameterized by Reynolds Number and angle of attack.

The unsteady incremental aerodynamics due to elastic deformation formulation is detailed in Ref. [11]. It is was built by using unsteady strip theory in time domain based on Jones' exponential approximation of Wagner's function [16].

The rigid–body state space model contains the classical three translational and three rotational equations of motion, plus three Euler's angles and three navigation equations (x, y and z coordinates), totalizing $n_{RB} = 12$ rigid–body state equations.

The four control surfaces and three motors were modeled with first–order dynamics, totalizing $n_a = 7$ actuator dynamic equations.

The aircraft structural-dynamic model contains elastic modes with frequencies up to $25Hz$, totalizing $n_e = 15$ elastic modes and $2n_e = 30$ state equations.

The incremental unsteady aerodynamic model was built by diving the lifting surfaces in strips with approximate length equal to $5cm$ totalizing $n_s = 110$ strips and $2n_s = 220$ aerodynamic lag state equations.

The number of state equations in the full–order model is then calculated as $n = n_{RB} + n_a + 2n_e + 2n_s = 269$.

5 Results

In the remaining of this paper, the following convention is used: Full–Order Model (FOM) refers to a model represented by equations (18) to (23); reduced–order model (ROM) refers to a model represented by equations (26) to (31). The number accompanying this nomenclature refers to the number of elastic modes that was used to represent the model, for example, FOM–15 refers to a model represented by equations (18) to (23) considering 15 elastic modes.

The model order reduction method presented in section 2 was applied to equations (22) and (23), retaining linear terms only. This is reasonable since we are interested in reducing simulation time by model order reduction and equation (23) contains the largest number of state equations. Additionally, equation (22) is responsible for introducing the highest frequency poles in the system, the influence of which may fastly vanish in time responses.

The rigid–body equations of motion and the actuator dynamics remain the same. The set of equations that describe the ROM is given by:

$$\dot{\boldsymbol{V}}|_B = -\boldsymbol{\omega}|_B \times \boldsymbol{V}|_B + \frac{1}{m}\left(\boldsymbol{T}_{BI}\boldsymbol{W}|_I + \boldsymbol{F}|_B\right) \tag{26}$$

$$\dot{\boldsymbol{\omega}}|_B = -\boldsymbol{J}^{-1}\left(\boldsymbol{\omega}|_B \times \boldsymbol{J}\boldsymbol{\omega}|_B\right) + \boldsymbol{J}^{-1}\boldsymbol{M}|_B \tag{27}$$

$$\dot{\boldsymbol{p}} = \boldsymbol{T}_{BI}^T \boldsymbol{V}|_B \tag{28}$$

$$\dot{\boldsymbol{\delta}} = -\boldsymbol{\tau}^{-1}\boldsymbol{\delta} + \boldsymbol{\tau}^{-1}\boldsymbol{u_c} \tag{29}$$

$$\begin{bmatrix}\dot{\boldsymbol{\eta}}(t)\\ \ddot{\boldsymbol{\eta}}(t)\end{bmatrix} = \boldsymbol{\Phi_e}\dot{\boldsymbol{z}}_{\boldsymbol{e}} + \overline{\boldsymbol{\Phi}}_{\boldsymbol{e}}\dot{\overline{\boldsymbol{z}}}_{\boldsymbol{e}} \tag{30}$$

$$\dot{\boldsymbol{\lambda}} = \boldsymbol{\Phi_a}\dot{\boldsymbol{z}}_{\boldsymbol{a}} + \overline{\boldsymbol{\Phi}}_{\boldsymbol{a}}\dot{\overline{\boldsymbol{z}}}_{\boldsymbol{a}}, \tag{31}$$

where

$$\dot{\boldsymbol{z}}_{\boldsymbol{e}} = \boldsymbol{A_e}\left(\boldsymbol{z_e} - \boldsymbol{z}_{e0}\right) + \boldsymbol{B_e}(\boldsymbol{u_e} - \boldsymbol{u}_{e0}), \tag{32}$$

and

$$\dot{\boldsymbol{z}}_{\boldsymbol{a}} = \boldsymbol{A_a}(\boldsymbol{z_a} - \boldsymbol{z}_{a0}) + \boldsymbol{B_a}(\boldsymbol{u_a} - \boldsymbol{u}_{a0}) \tag{33}$$

where $\boldsymbol{z_a}$ and $\boldsymbol{z_e}$ are the reduced–order state variables; $\boldsymbol{u_e}$ and $\boldsymbol{u_a}$ contain the relevant variables that describe the flight conditions at a given time instant; $\boldsymbol{z}_{e0}$, $\boldsymbol{z}_{a0}$ are calculated as

$$\boldsymbol{z}_{e0} = \boldsymbol{\Psi}_{\boldsymbol{e}}^T[\{\boldsymbol{\eta}_0\}\{\dot{\boldsymbol{\eta}}_0\}]^T \tag{34}$$

and

$$\boldsymbol{z}_{a0} = \boldsymbol{\Psi}_{\boldsymbol{a}}^T\boldsymbol{\lambda}_0 \tag{35}$$

The ROM–7 basis is composed by the seven lowest frequency structural modes (modes up to $12.9Hz$ were considered) plus four aeroelastic lag states, two for the wing and two for the tails. Figure 2 illustrates the map of poles for both, FOM–15 and ROM–7. Besides FOM–15, in order to compare simulation results of a FOM and a ROM with the same number of elastic modes taken into account, simulations with a FOM–7 are presented as well.

The simulations were performed in a computer equipped with a microprocessor Intel Core

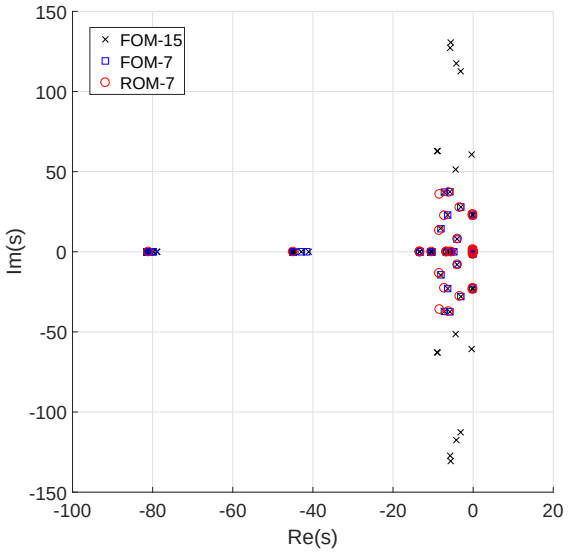

Fig. 2 Map of poles of Full–order models and Reduced–order model

i7–7700HQ 2.8GHz, 8GB of RAM, *Windows 10* and *MATLAB 2017a*. The time integration algorithm used was the fixed–step, fourth–order Runge–Kutta method and the time steps were chosen according to the criterion of representing the highest frequency of each model with 8 points per cycle. Table 1 summarizes this criterion.

Two test cases are presented, in both the operation velocity and altitude are $14m/s$ and $650m$, respectively.

In the first test case, a three–degree elevator doublet command was applied in order to compare the FOM and ROM longitudinal time responses. Figure 3 shows the elevator deflection; Figure 4 shows the wing tip displacements and Figure 5 illustrates the longitudinal response of the aircraft and Figure 6 shows the coupled lateral–directional response, , because the aircraft has its center of gravity slightly offset to the left. Another relevant characteristic to fully understand the lateral–directional behavior in Figure 6 is that the aircraft has elevator roll control reversal.

The second test case consists in a frequency sweep, ranging from $0.5Hz$ to $2.5Hz$, applied to the ailerons, as seen in Figure 7. Figures 8 and 9 illustrate wing tip displacements and the lateral–directional responses, respectively. Particularly, in Figure 8, the small but persistent difference in wing tip displacements between FOM-15 and FOM-7 is due to the different number of elastic modes retained in both – this difference is also present in Figure 4.

Through the analysis of Figure 3 to 9, it is possible to observe that the proposed ROM was capable of approximating the FOM for both longitudinal and lateral–directional dynamics. With respect to the simulation times, Table 2 compares the average simulation time for a *10s* flight.

Model	$\overline{T_s}$ [s]	Standard deviation
FOM–15	7.95	0.04
FOM–7	4.71	0.02
ROM–7	2.84	0.02

Table 2 Average simulation computational time for a 10s flight calculated through 5 samples.

Through the analysis of Table 2, it is possible to observe that ROM–7 provided a simulation computational time reduction of 64.23% when compared with FOM–15 and 39.6% when compared with FOM–7.

6 Concluding Remarks

This paper presented an approach based on reduced–order models for reducing computational cost of flexible aircraft simulations.

A model order reduction technique that uses information on the eigenspectrum of the Jacobian matrix and projects the system through a Taylor series expansion onto a small basis of eigenvectors was applied to the aeroelastic and aerodynamic lag state equations while the rigid–body equations of motion were unchanged. Automatic differentiation algorithms were employed to obtain the reduced-order model matrices.

The results show a good agreement between full–order–models and reduced–order–model, with a significant reduction of computational cost when using the latter.

Moreover, the reduced-order model was shown to be able to yield in much less computing time results that are in good agreement with

	FOM–15	FOM–7	ROM–7
Number of Elastic Modes	15	7	7
Highest frequency pole [Hz]	20.81	12.9	12.9
Time step [ms]	6	10	10

Table 1 Simulation time step.

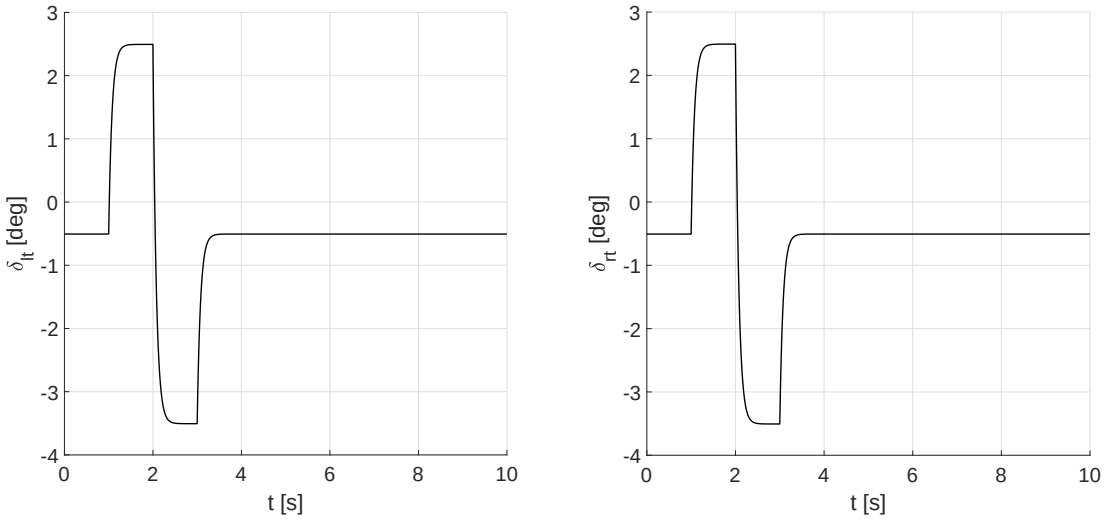

Fig. 3 Left and right elevator deflection for a 3 degree doublet.

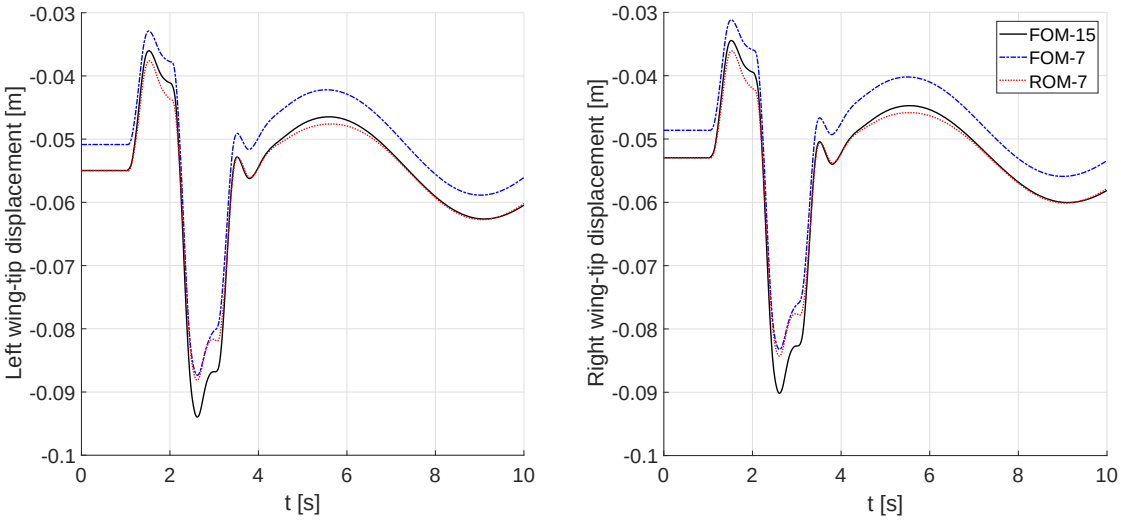

Fig. 4 Wing tip displacements (positive downwards) due to a 3 degree elevator doublet.

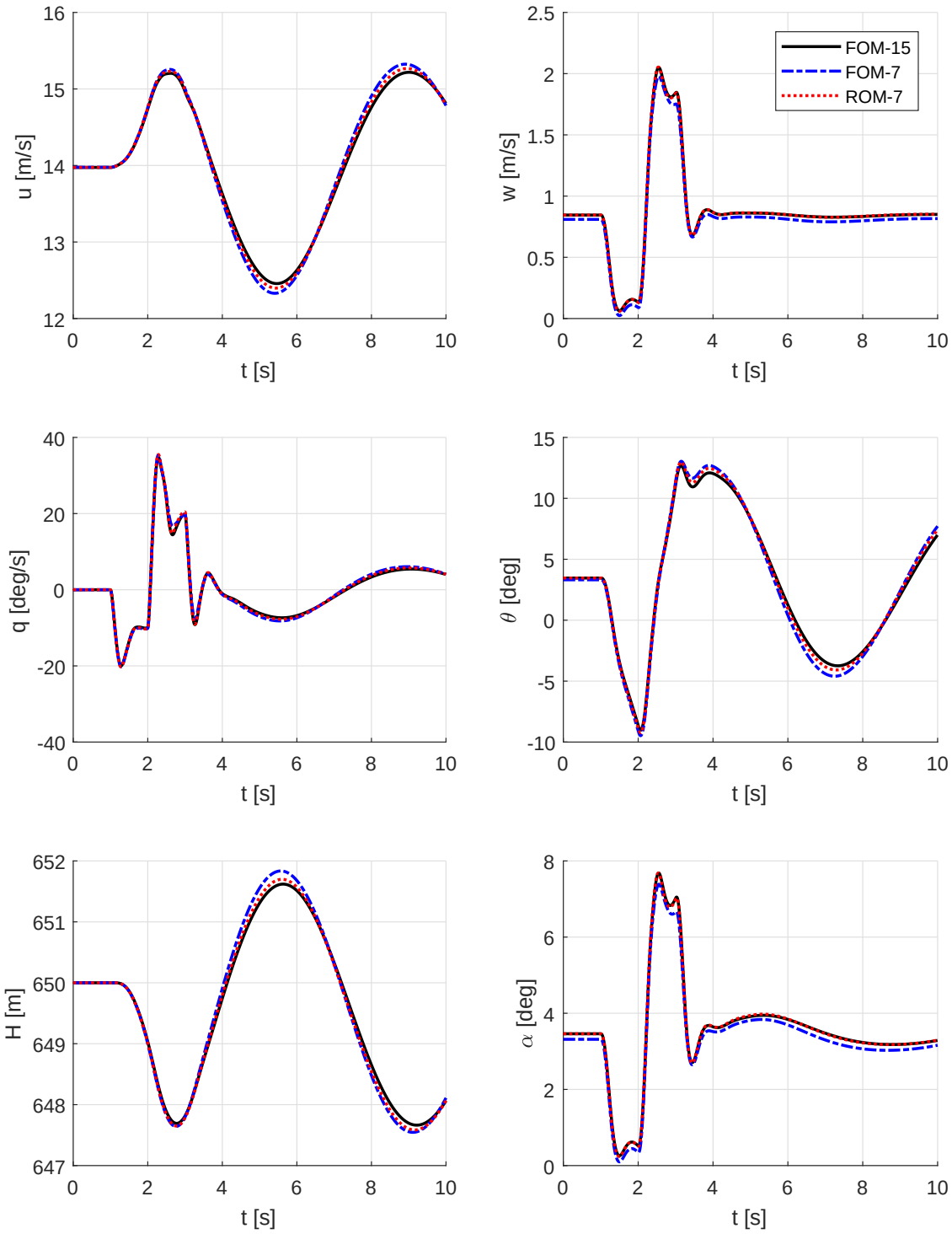

Fig. 5 Longitudinal response due to a 3 degree elevator doublet.

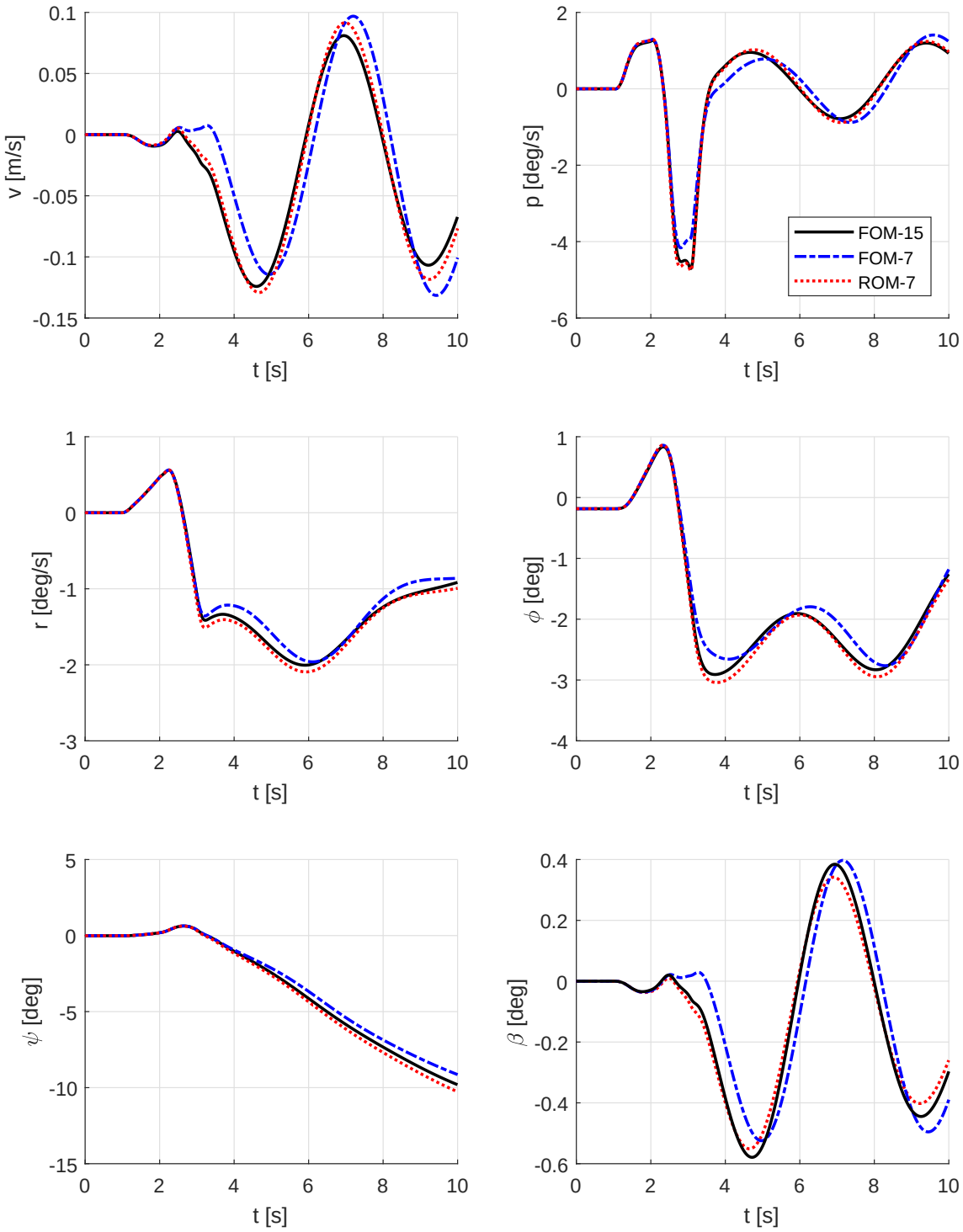

Fig. 6 Lateral-directional response due to a 3 degree elevator doublet.

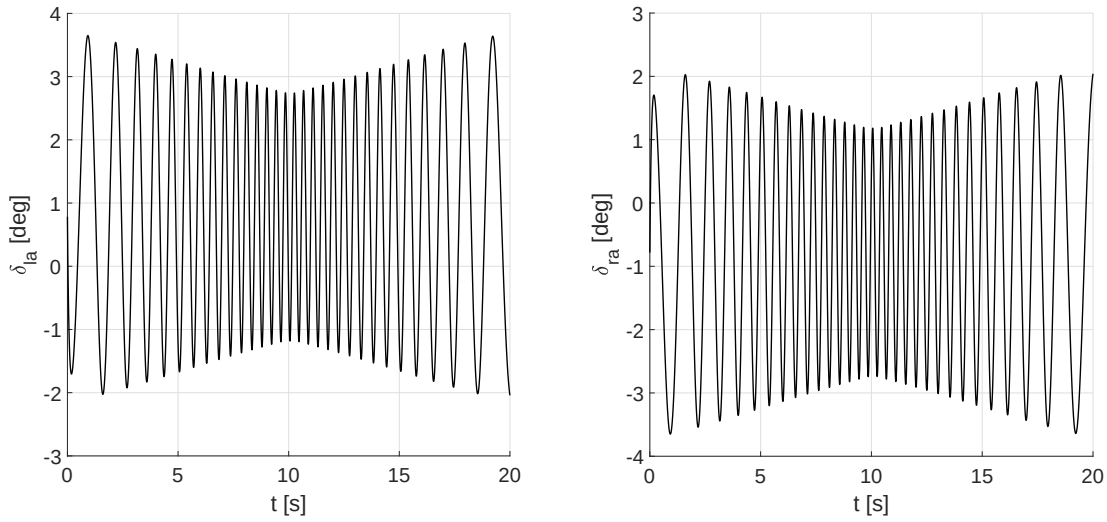

Fig. 7 Left and right ailerons deflection for a 0.5 Hz to 2.5 Hz frequency sweep command.

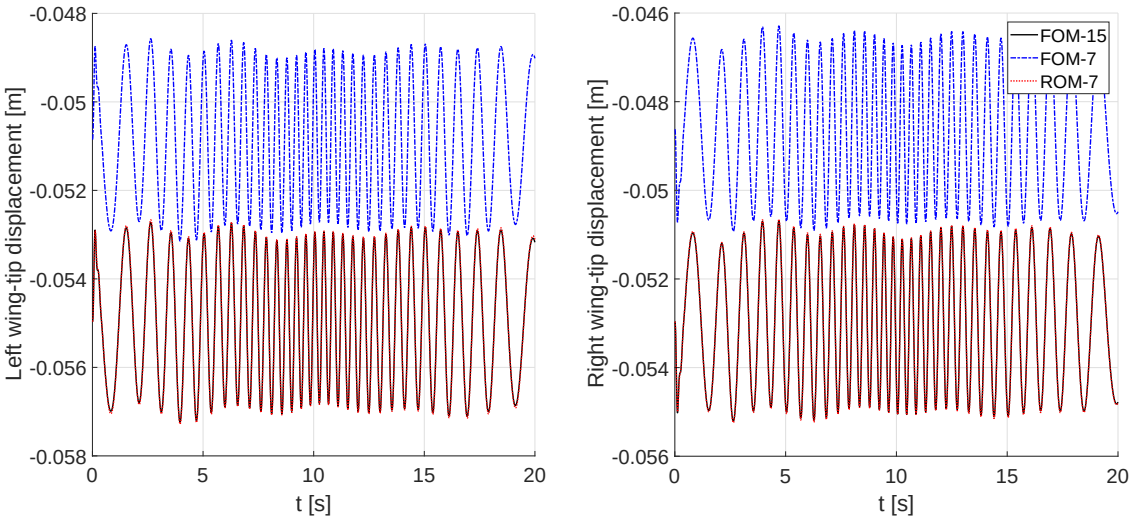

Fig. 8 Wing tip displacements (positive downwards) due to a 0.5 Hz to 2.5 Hz frequency sweep

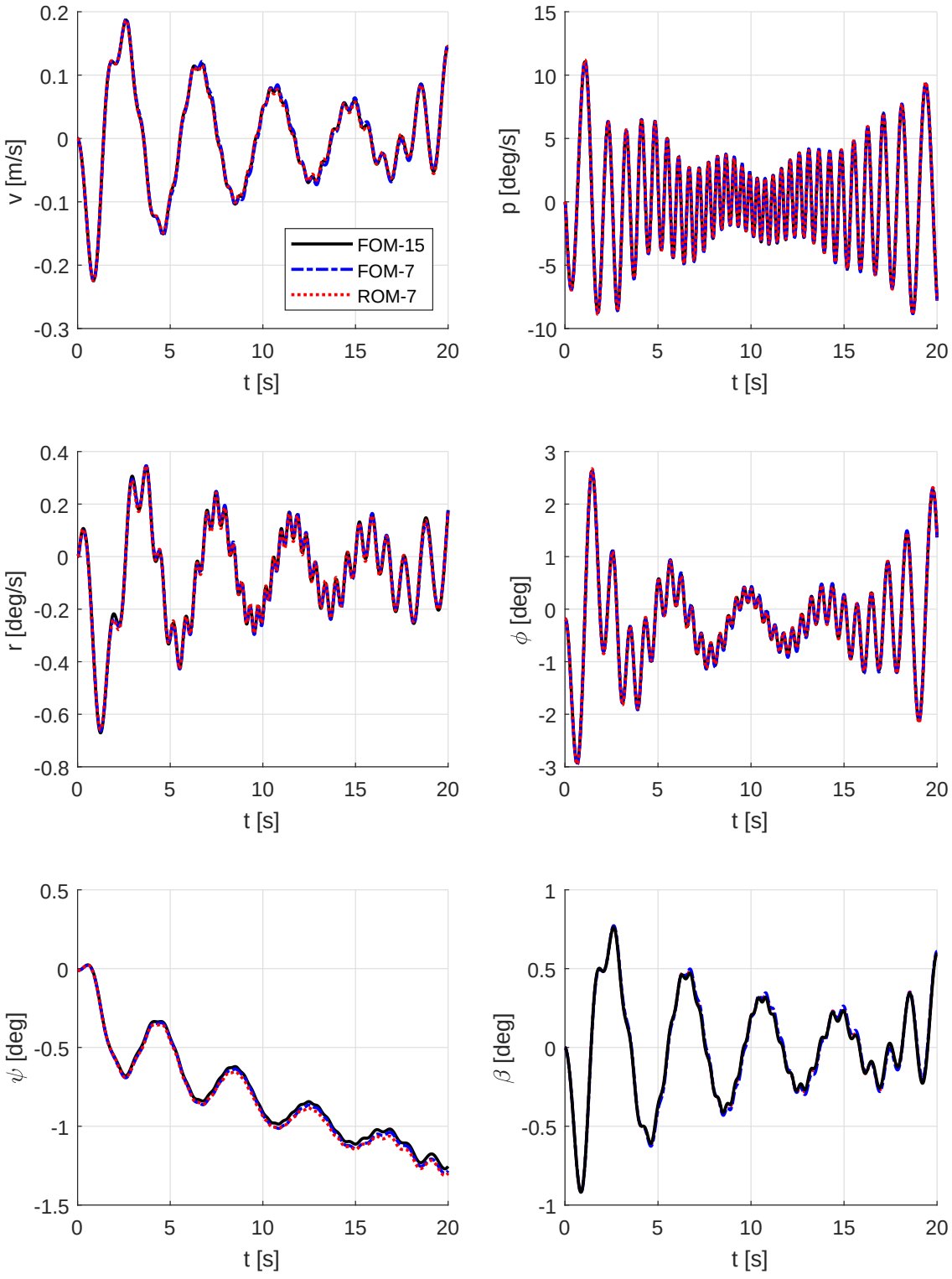

Fig. 9 Lateral-directional response due to a 0.5 Hz to 2.5 Hz frequency sweep.

those provided by a full-order model having the same number of elastic degrees of freedom.

The findings and discussions are conservative and the advantages provided by the proposed approach may become larger when dealing with models that include structural-dynamic or incremental aerodynamic nonlinearities or both.

References

[1] Livne E. Future of Airplane Aeroelasticity, *Journal of Aircraft*, Vol. 40, No. 6, pp.1066-1092, 2003.

[2] Shearer C M and Cesnik C E S. Nonlinear Flight Dynamics of Very Flexible Aircraft, *AIAA Atmospheric Flight Mechanics Conference and Exhibt*, AIAA paper 2005-5805, 2005.

[3] Guimarães Neto A, Silva R G A, Paglione, P and Silvestre, F J. Formulation of the Flight Dynamics of Flexible Aircraft Using General Body Axes, *AIAA Journal*, Vol. 54, No. 11, 2016.

[4] Kaden A, Boche B and Luckener R. Hardware-in-the-loop flight simulator - an essential part in the development process for the automatic flight control system of a utility aircraft. *Advances in Aerospace Guidance, Navigatin and Control*, Springer, Berlin, pp. 585-601, 2013.

[5] Waszniowski L, Hanzalek Z, and Doubrava J. Aicraft control system validation via hardware-in-the-loop simulation. *Journal of Aircraft*, Vol.48, No.4, pp. 1466-1468, 2011.

[6] González P, Boschetti P, Cárdenas E. and Amerio A. Evaluation of the flying qualities of a half-scale unmanned airplane via flight simulation. *48th AIAA Aerospace Sciences Meeting Including the New Horizons Forum and Aerospace Exposition*, Florida, AIAA paper 2010-298, 2010.

[7] Kish B A, Leggett D B, Nguyem B T, Cord T J, Slutz G J. Concepts for detecting pilot-induced oscillation using manned simulation.*21st Atmospheric Flight Mechanics Conference, Guidance, Navigation, and Control and Co-located Conferences*, pp. 559-568, 1996.

[8] Da Ronch A, Badcock K, Wang Y, Wynn A and Palacios R.Nonlinear Model Reduction for Flexible Aircraft Control Design, *AIAA Atmospheric Flight Mechanincs Conference*, AIAA Paper 2012-4404, 2012.

[9] Patterson M A, Weinstein M, Rao A V. An efficient overloaded method for computing derivatives of mathematical functions in MATLAB, *ACM Transactions on Mathematical Software*, Vol. 39, No. 3, pp 17:1–17:36, 2013.

[10] Cesnik C E S, Senatore P J, Su W and Atkins E M. X-HALE: A Very Flexible Unmanned Aerial Vehicle for Nonlinear Aeroelastic Tests, *AIAA Journal*, Vol. 50, No. 12, December 2012.

[11] Silvestre F J. *Methodology for Modeling the Dynamics of Flexible, High-Aspect-Ratio Aircraft in the Time Domain for Aeroservoelastic Investigations*, 1st ed., Mensch and Buch Verlag, 2013.

[12] Silvestre F J and Luckner R. Experimental Validation of a Flight Simulation Model for Slightly Flexible Aircraft, *AIAA Journal*, Vol. 1, No. 1, pp.1-17, 2015.

[13] Waszak M R and Schmidt D K. Flight Dynamics of Aeroelastic Vehicles, *Journal of Aircraft*, Vol. 25, No. 6, pp.563-71, 1988.

[14] Hedman S G. Vortex Lattice Method for Calculation of Quasi Steady State Loadings on Thin Elastic Wings, *Aeronautical Research Inst. of Sweden Rept. 105*, Stockholm, 1965.

[15] Drela M. XFOIL: An analysis and design system for low reynolds number airfoils, In Mueller T., *Low Reynolds Number Aerodynamics*, Vol. 54 of *Lecture Notes in Engineering*, pp. 1-12, Springer, Berlin Heidelberg, 1989.

[16] Wagner H. Über die Entstehung des dynamischen Auftriebes von Tragflügeln, *Zeitschrift für angewandte Mathematik und Mechanik 5*

Contact Author Email Address

paulino.juliano@gmail.com

Acknowledgement

This work has been funded by FINEP and EMBRAER under the research project Advanced Studies in Flight Physics, contract number 01.14.0185.00.

Da Ronch gratefully acknowledges the financial support from the Engineering and Physical Sciences Research Council (grant number: EP/P006795/1) and from the University of

Southampton Global Partnerships Award 2017-18.

Copyright Statement